



Research paper

Mechanical characteristics of ultra-shallow buried high-speed railway tunnel in broken surrounding rock during construction

Shaoju Hao¹, Ruizhen Fei², Jia Yu³

Abstract: The mechanical state of broken surrounding rock during the construction of ultra-shallow buried high-speed railway tunnel is very complicated, seriously affecting the construction safety. Taking Huiyong Xishan tunnel on Beijing-Shenyang Line as engineering background, MADIS/GTS NX numerical simulation and field test methods are used to analyze the characteristics of stress field, overall displacement, horizontal convergence of tunnel sidewalls and vault settlement during construction. The main mechanical characteristics of ultra-shallow buried high-speed railway tunnel with broken surrounding rock include: (1) After the stress redistribution, the stress concentration occurs at the boundary of the tunnel sidewall and surrounding rock, and the vertical displacement of tunnel vault and bottom appears obviously. (2) The horizontal displacement on both sides of the initial lining is obvious, while the horizontal displacement on the upper and lower support is small. The maximum lateral displacement of the initial lining is 1.71 cm, while the maximum vault settlement of the lower invert is 9.3 cm. (3) Both the horizontal convergence and the vault settlement increase with time. The growth rate is large in the early stage and tends to be stable in the later stage. (4) Compared with exponential and hyperbolic functions, the logarithmic function is most suitable for regression analysis of horizontal convergence and measured vault settlement data, and its fitting accuracy is higher than 90%.

Keywords: broken surrounding rock, ultra-shallow buried, high-speed railway tunnel, numerical simulation, deformation characteristics

¹Prof., MSc., Eng., Henan Radio & Television University, Zhengzhou, 450046, China, e-mail: haoshaoju2021@163.com, ORCID: 0000-0002-2091-3320

²DSc., PhD., Eng., Central South University, Changsha, 410075, China, e-mail: feiruizhen@crdc.com, ORCID: 0000-0002-9142-4890

³MSc., Eng., Zhenhua Port Machinery Co. LTD, Shanghai, 200125, China, e-mail: yuj202203@163.com, ORCID: 0000-0001-6690-6786

1. Introduction

With the rapid development of China's economy and the continuous expansion of the national high-speed railway network, tunnels with their unique advantages are gradually understood and recognized by people, including some ultra-shallow tunnels through broken surrounding rocks [1–6]. According to the specification [7], when the thickness of soil covering the upper part of the tunnel is less than the calculation height of vertical load, the tunnel should be designed as an ultra-shallow buried tunnel. When the buried depth of high-speed railway tunnel reaches ultra-shallow buried tunnel standard and the surrounding rock state is broken and discrete, the stress state of the surrounding rock will become extremely unstable, and the probability of construction risks such as roof falling, collapse, deformation instability, and mountain cracking will increase [8–10]. Analysis of deformation and stress characteristics in the construction process of ultra-shallow buried high-speed railway tunnel with broken surrounding rock is a necessary premise to ensure the safety of this kind of tunnel construction.

In recent years, scholars have actively researched the mechanical characteristics of excavation and the stability of the excavation face of the tunnel buried in broken soft surrounding rock in the construction process. Chen, et al. [11] described a case study on the supporting method and large deformation mechanism. The Maoxian tunnel in Sichuan Province constructing in soft-weak rock masses was involved and a comparative was carried out against the internal stress of the steel arch, supporting mechanism of surrounding rock and bending moment and axial force of the secondary lining. Hisatake and Hieda [12] derived a 3D back analysis method to calculate the mechanical properties of surrounding rock in front of the palm face and verified the accuracy and effectiveness of the 3D back analysis method by using finite element method. Alagha and Chapman [13] used numerical simulation method to analyze the stability of roadway face with uniform layered soft soil foundation. The arching effect was studied and the failure mechanism of roadway face under different conditions was proposed. Shao, et al. [14] took Yangshan tunnel as the engineering background and used FLAC 3D software to analyze the influence of fault fracture zone on the stability of tunnel excavation. Wu, et al. [15] analyzed the failure mechanism of tunnel vault in soft surrounding rock by combining numerical simulation with a model test. Xu, et al. [16] studied the evolution of surrounding rock and the gradual process of collapse failure in the condition that there was no fault above the vault in class IV surrounding rock by using finite element method and test method.

Although academics have used finite element method, scale tests, and field tests to study the mechanical characteristics of excavation and the stability of the tunnel excavation face, a series of achievements have been obtained which are valuable for engineering construction. However, there are few pieces of research to analyze the deformation and stress characteristics of ultra-shallow buried high-speed railway tunnel in broken surrounding rock during construction. Taking Huying Xishan tunnel under construction on Beijing-Shenyang Line as the engineering background, MIDAS/GTS NX software is used to analyze the load and deformation characteristics of ultra-shallow buried high-speed railway tunnel in broken surrounding rock during construction.

2. Engineering background

Huying Xishan tunnel is one of the key tunnel projects of the Beijing-Shenyang Line. The starting and ending mileage of the tunnel is DIK 147+997 and DIK 159+329, with a total length of 11332 m, and the maximum buried depth is 376.5 m. Huying Xishan tunnel is a double-track single-hole tunnel. The longitudinal gradient is one-way and the gradient is 2%. The mileage DIK 151+000~DIK 157+000 section has a downhill gradient of 1.49%, and the mileage DIK 157+000~DIK 159+300 section has a downhill gradient of 0.3%. The mileage of the slope section is DIK 159+300~DIK 159+329. The project adopts a composite lining structure, with a maximum net width of 13.3 m and a net height of 9.82 m after construction.

The excavation section of Huying Xishan tunnel is large, and the surrounding rock grade of mileage DIK 158+993~DIK 159+037 section is V, the geological conditions are poor, and the main adverse geological conditions include ultra-shallow burial, fault fracture zone, etc. As shown in Fig. 1, the national road and original river is indicated by the red arrow. The topographic site photo of this section shows that the minimum buried depth of the top of the tunnel is -1.7 m, the top of the tunnel is exposed. The tunnel intersects obliquely with the original river at an angle of approximately 70° and the national highway at an angle of approximately 60° . Most of the precipitation in the mountain area is collected by the bottom of the riverbed. The figure shows that the precipitation collecting path passes through the tunnel, indicating that the area is rich in underground water. The detailed survey data show that the geological condition here is poor and collapse accidents are very easy to occur. Given the unfavorable geological conditions in the ultra-shallow buried section of mileage DIK 158+993~DIK159+037, the three-bench temporary transverse support method is adopted for construction. The main processes include: excavating upper bench, initial support, installation of the temporary transverse support, excavating middle bench, driving anchor rods, closing inverted arch, excavating lower bench, closing inverted arch, etc. Fig. 2 shows the construction process of three-bench temporary transverse support method.



Fig. 1. Topographic site photo

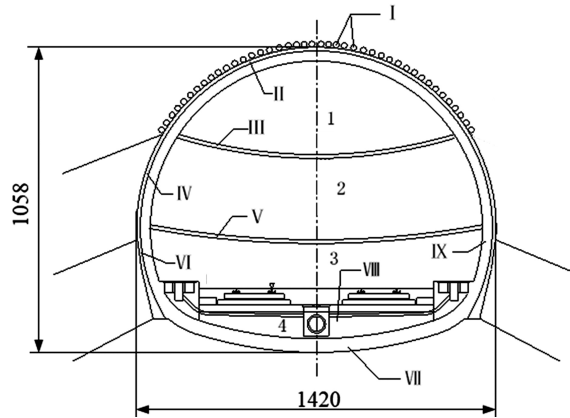


Fig. 2. Schematic diagram of the cross-section of three-bench temporary transverse support method (unit: cm)

3. Research methods

3.1. Field measurement

Monitoring points of vault settlement and horizontal convergence are set at mileage DIK 159+003, DIK 159+008, DIK 159+018, and DIK 159+025, and surface settlement monitoring points are set at sections DIK 159+005 and DIK 159+015. The layout of measuring points is shown in Fig. 3. The horizontal distance of surface settlement measuring points is 6 m. The settlement points of the arch crown are arranged at the position of the arch crown, and the two horizontal convergence measuring points along the tunnel center line are symmetrically arranged at the same vertical height.

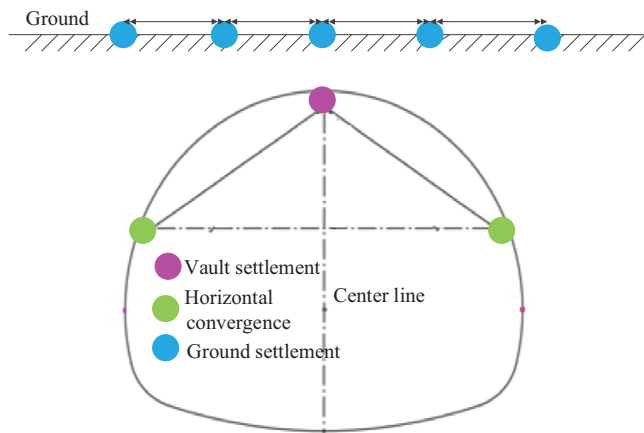


Fig. 3. Schematic diagram of measuring point layout

3.2. Regression analysis method of measured data

Regression analysis is an important method to understand the construction characteristics and time behavior during tunnel construction, which can be used to study the deformation law, predict the maximum deformation and change rate of the tunnel. There are three kinds of mathematical functions, exponential function, logarithm function, and hyperbolic function, which are usually used in the regression analysis of tunnel construction displacement time history. The applicability of the three regression models needs to be studied because of the complex mechanical properties of the ultra-shallow tunnel in the broken surrounding rock. The three regression analysis functions are summarized as follows.

1. Exponential function:

$$U = Ae^{-B/t},$$

2. Logarithmic function:

$$U = A \lg(1 + t) + B,$$

3. Hyperbolic function:

$$U = t(A + Bt),$$

where U is the deformation or stress; A and B are regression coefficients; t is the observation time of the measuring point.

3.3. Numerical simulation method

The construction and excavation process of ultra-shallow buried tunnel section from mileage DIK 158+993 to DIK 159+037 is analyzed, and the length along the tunnel direction is 44 m. To eliminate the effect of boundary effect, the transverse size of the model is 90 m, the tunnel bottom invert is taken 34 m downward, and the tunnel vault is taken up to the surface. According to the geological conditions and construction conditions of Huying Xishan tunnel, the numerical model is established, and the model size ($X \times Y \times Z$) is 90 m \times 40 m \times 70 m. In the initial stage of the model, solid elements are selected for supporting structure, arch, and surrounding rock, plate elements are used for secondary lining and temporary transverse support, and equivalent reinforcement rings are used for large pipe shelters and small leading pipes. To improve the modeling efficiency, the spatial surface structure of temporary transverse support is ignored and simplified to a flat plate structure. The total number of model elements is 166515, and the total number of nodes is 193091. The normal constraint is selected on the side, the translational freedom in the three directions is defined on the bottom, and the free boundary is set on the top. The established tunnel model and supporting structure are shown in Fig. 4.

3D solid element is used to simulate the initial support. The double-layer steel mesh set in the initial support construction is regarded as the safety reserve and is not involved in the calculation during the model analysis in this paper. Steel arch and shotcrete are combined as one component in the model, and the elastic modulus of steel arch itself is converted

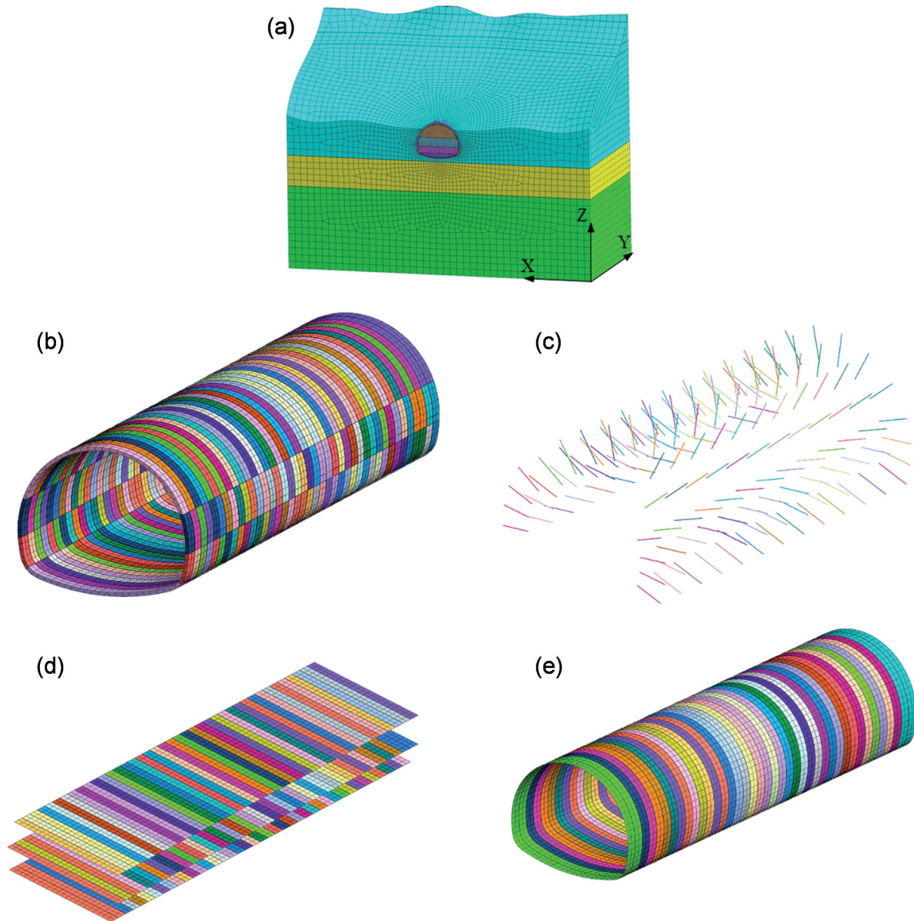


Fig. 4. Finite element model of the tunnel: (a) Overall model; (b) Initial support; (c) Anchor rod; (d) Temporary transverse support; (e) Secondary lining

into shotcrete according to Eq. (3.1):

$$(3.1) \quad E = E_0 + \frac{S_g + E_g}{S_c}$$

where, E is the elastic modulus of concrete after conversion; E_0 is the elastic modulus of the original concrete and $E_0 = 31.5$ GPa; E_g is the elastic modulus of steel arch, and $E_g = 210$ GPa; S_g is the cross-section area of steel arch, and $S_g = 48.28$ cm²; S_c is the cross-sectional area of shotcrete and $S_c = 3000$ cm².

According to the Eq. (3.1), $E = 34.38$ GPa. The remaining parameters are determined according to tunnel geological survey data and are shown in Table 1.

Table 1. Calculation parameters

Materials	Unit weight (kN/m ³)	Elasticity modulus (GPa)	Poisson's ratio	Cohesive force C (kPa)	Internal friction (°)
Coarse breccias soil	22	0.05	0.36	60	17
Pebbles soil	24	0.3	0.28	0	25
Quartz trachyte	25	0.9	0.27	230	27
Initial support	23	34.4	0.2	–	–
Secondary lining	25	31.5	0.2	–	–
bolt	24	31.5	0.2	–	–
Temporary transverse support	78.5	210	0.2	–	–
Large pipe shed	23	34.4	0.2	–	–
Advance small catheter	23	34.4	0.2	–	–

3.4. Validation

To verify the correctness of the numerical simulation method, Fig. 5 compares the measured settlement displacement and the numerical simulation at 4 measuring points of DIK 159+005 and DIK 159+015 sections. As shown in Fig. 5, the distribution characteristics of numerical simulation results are the same as those of field measured data. The maximum error of numerical simulation results of DIK 159+005 and DIK 159+015 sections is only 0.26 cm and 0.14 cm, indicating that the numerical model established in this paper has high accuracy.

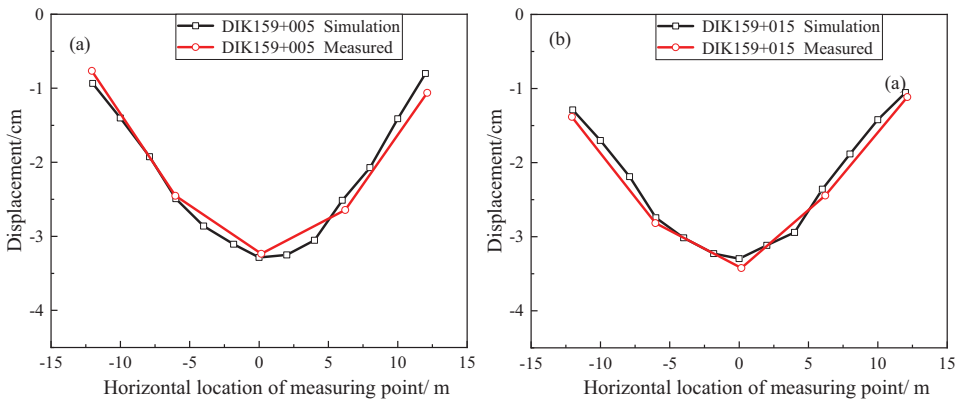


Fig. 5. Verification of numerical results: (a) DIK159+005; (b) DIK159+015

4. Mechanical characteristics during construction

4.1. Surrounding rock

The rock mass will produce a certain amount of settlement under the action of dead weight, but it has already reached a stable state due to the long-term consolidation process. Therefore, the displacement of rock mass should be cleared and the dead weight stress of rock mass should be calculated as the initial stage of tunnel excavation. MIDAS GTS NX finite element model soil gravity stress balance cloud diagram is shown in Fig. 6.

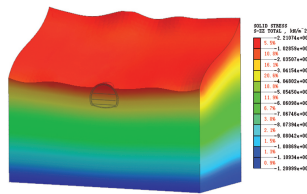


Fig. 6. Gravity stress balance (unit: kPa)

Fig. 7 shows the stress field of the upper bench excavation at 12 m, 24 m, and the completion of excavation. As can be seen from Fig. 7, the original stress state of rock mass is broken by tunnel excavation, and the stress began to be redistributed along the excavation surface. After stress redistribution, the tunnel surrounding rock reached a new stress balance. It can be seen from Fig. 7 that stress concentration occurs in both horizontal and vertical directions at the boundary between the tunnel sidewall and surrounding rock.

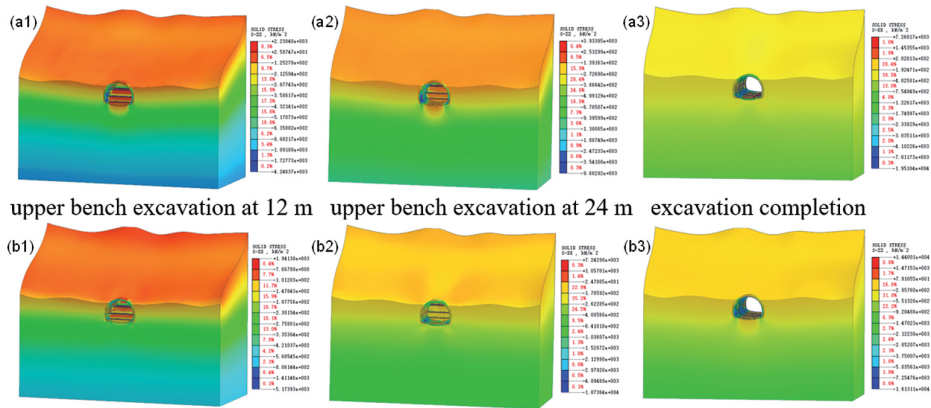


Fig. 7. Stress contour of tunnel excavation at different stages (unit: kPa):
 (a) X direction; (b) Z direction

The excavation area and sequence of each part are simulated according to the temporary horizontal brace method of three steps, and the construction process is simulated by construction steps. Fig. 8 shows the overall displacement of surrounding rock after exca-

vation of upper bench. As shown in Fig. 8, the tunnel and its upper and lower rock mass show obvious vertical displacement. The displacement direction of the tunnel bottom is mainly vertical upward, the displacement direction of the surrounding rock of the vault is vertical downward, and the vertical displacement of the surrounding rock of the tunnel top near the tunnel exit is small. In the process of tunnel excavation, the vertical displacement mainly occurs in the arch roof and the arch bottom, and the vault settlement is much larger than the vertical settlement of surrounding rock. This phenomenon is caused by the dead weight and extrusion of the surrounding rock. After the tunnel excavation, the initial stress state of the surrounding rock is destroyed, and the dead weight of the surrounding rock makes the surrounding rock tend to squeeze into the tunnel, thus resulting in a large vertical displacement.

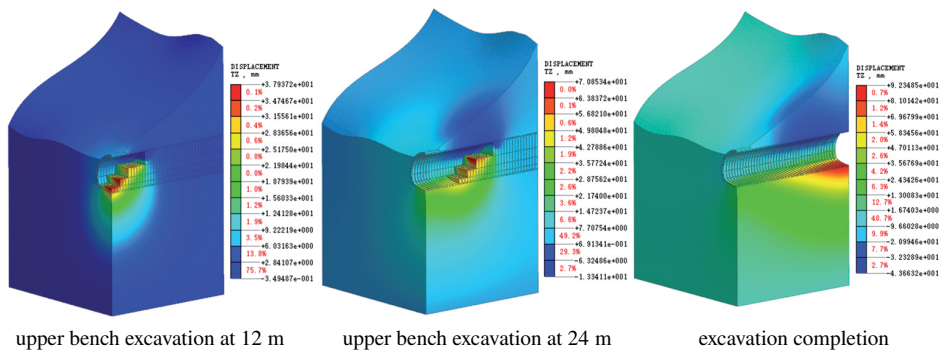


Fig. 8. Displacement contour of the tunnel (unit: mm)

4.2. Initial lining and inner support

The stresses in X and Z directions of initial lining calculated by numerical analysis are shown in Figs. 9 and 10.

It can be seen from Fig. 9 that the initial lining is dominated by compression, the compressive stress value is much larger than the tensile stress value, and the maximum horizontal compressive stress location is at the vault. When the upper bench is excavated to 3 m, the maximum horizontal compressive stress of initial lining appears at the vault, which is 1.27 MPa. When the upper bench excavation reaches 6 m, the maximum horizontal compressive stress of initial lining appears at the vault, which is 2.28 MPa. When the middle bench is excavated to 3 m, the maximum horizontal compressive stress of initial lining appears at the vault, which is 4.42 MPa. When excavated to 3 m, the maximum horizontal compressive stress of initial lining appeared at the vault, which is 5.17 MPa.

It can be seen from Fig. 10 that the maximum vertical compressive stress of the initial lining occurs at the connection with the steel transverse support during excavation. When the upper bench is excavated to 3 m and 6 m, the maximum stress is 2.06 MPa and 4.57 MPa, respectively. When the middle bench is excavated to 3 m, the maximum vertical stress is 6.73 MPa. When the lower bench is excavated to 3 m, the maximum vertical stress is 8.66 MPa.

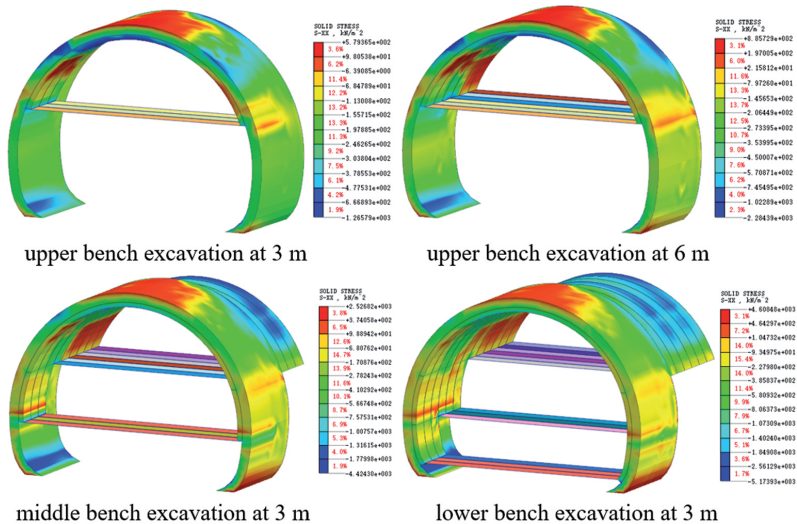


Fig. 9. Stress of initial lining in X direction

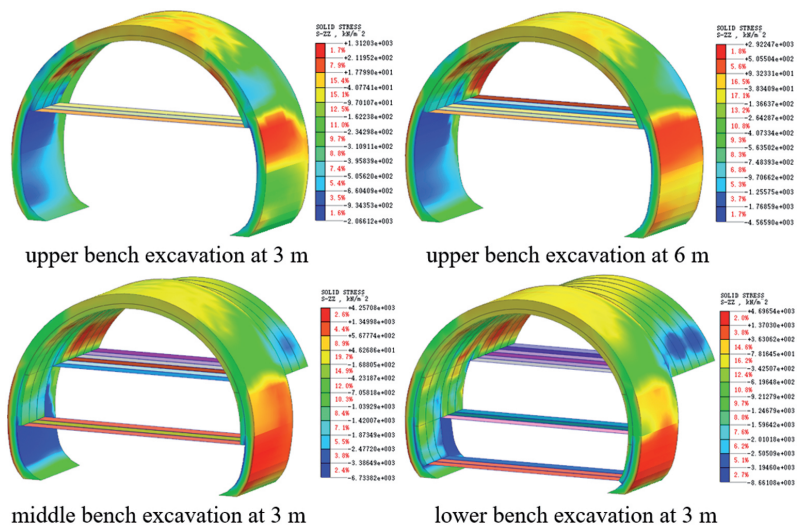


Fig. 10. Stress of initial lining in Z direction

Fig. 11 shows the displacement field in X and Z directions of initial lining after excavation. As shown in Fig. 11a, due to the vertical compression of surrounding rock, obvious horizontal displacement occurs on the left and right sides of the initial lining, while the horizontal displacement of the upper and lower support is small. The maximum horizontal displacement of the initial branch is 1.71 cm. Fig. 11b shows the displacement cloud diagram in the Z direction of the initial lining, in which the upper part of the support structure presents obvious settlement displacement with the maximum settlement value of

4.2 cm, while the lower part of the support close to the invert shows a large uplift with the maximum uplift of 9.3 cm. This phenomenon is also caused by the dead weight and extrusion of surrounding rock.

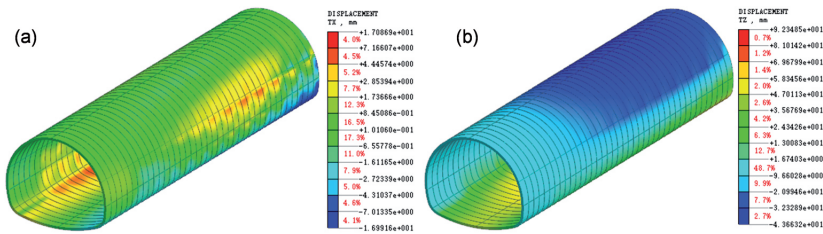


Fig. 11. Displacement field of initial lining (unit: m): (a) X direction; (b) Z direction

4.3. Field monitoring results

The numerical simulation results show that the stress concentration phenomenon is easy to occur at the boundary between the tunnel sidewall and surrounding rock during the excavation process, and the vertical displacement of surrounding rock mainly occurs at the vault and the bottom of the arch. Therefore, the horizontal convergence and the settlement of the vault are continuously monitored during the construction process. Horizontal convergence and vault settlement curves of four sections at mileage DIK 159+003, DIK 159+008, DIK 159+018, and DIK 159+025 are shown in Figs. 12 and 13.

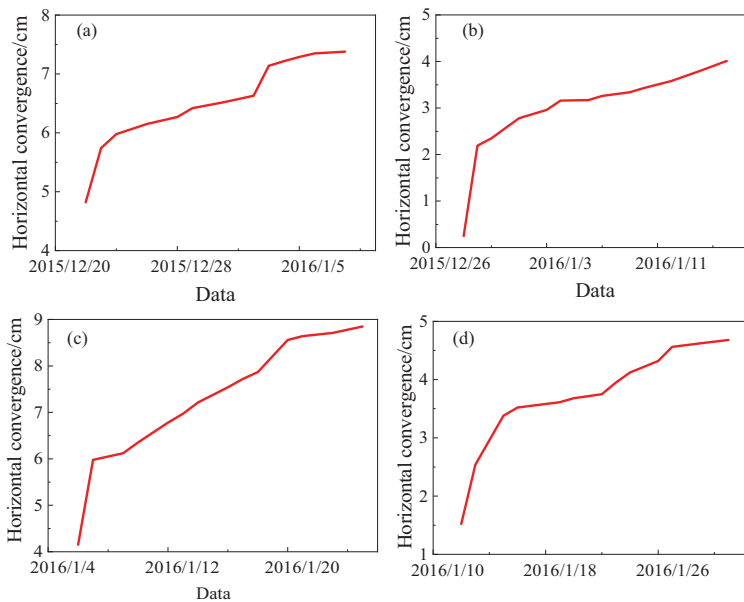


Fig. 12. Field measurement results of horizontal convergence of tunnel sidewalls: (a) DIK 159+003; (b) DIK 159+008; (c) DIK 159+018; (d) DIK 159+025

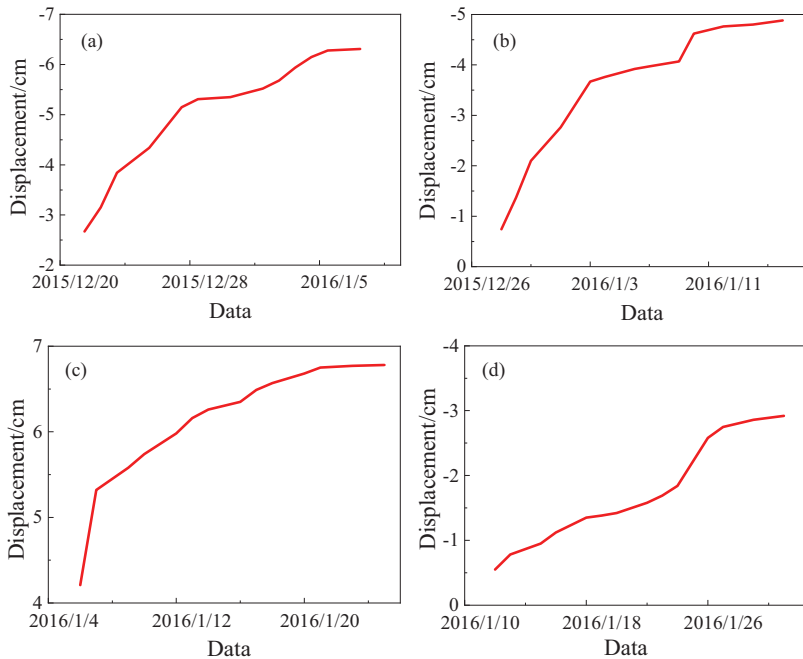


Fig. 13. Field measurement results of settlement of tunnel vault: (a) DIK 159+003; (b) DIK 159+008; (c) DIK 159+018; (d) DIK 159+025

It can be seen from Figs. 12 and 13 that both horizontal convergence and vault settlement increase with time during the excavation of ultra-shallow buried high-speed railway tunnel in the broken surrounding rock, and the growth rate is large in the early stage (i.e., the slope of the curve is large), and the growth rate tends to be stable in the later stage. This is because the initial stress field of surrounding rock is destroyed in the early stage of excavation, and the earth pressure suddenly acted on the initial support structure, leading to a sharp increase in the convergence rate. However, in the late stage of initial support forming, the earth pressure is borne by the steel arch, and the tunnel convergence rate gradually slowed down. After the excavation, the maximum values of horizontal convergence and vault settlement are located at the section of DIK 159+003, which are 7.6 cm and 6.3 cm, respectively.

4.4. Regression analysis

Taking DIK 159+003 and DIK 159+018 as examples, the data of horizontal convergence and vault settlement are substituted into three different regression analysis models respectively, and the regression analysis is conducted by using the least square method. The results are shown in Figs. 14 and 15. In the figures, r represents the correlation coefficient. The closer the absolute value of r is to 1, the greater the correlation degree is and the higher the regression accuracy is.

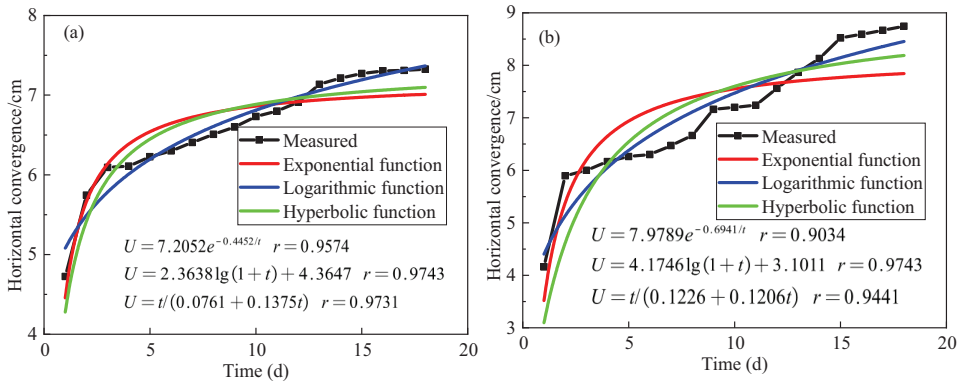


Fig. 14. Regression analysis of horizontal convergence of tunnel sidewalls:
 (a) DIK159+003; (b) DIK159+018

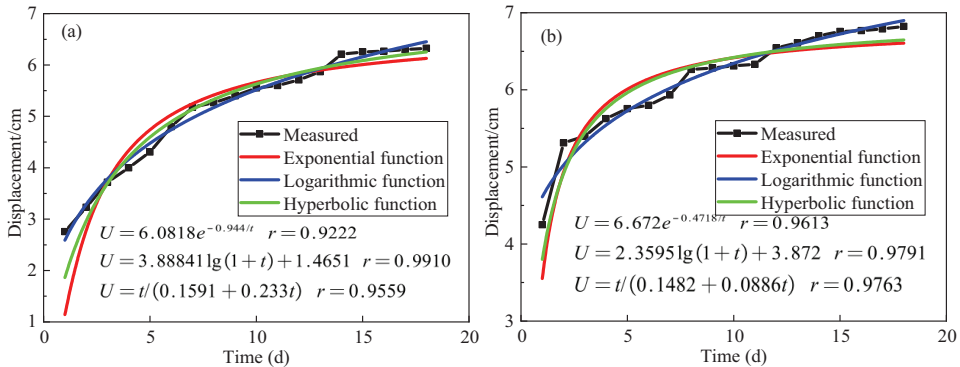


Fig. 15. Regression analysis of the settlement of tunnel vault:
 (a) DIK159+003; (b) DIK159+018

It can be seen from Figs. 14 and 15 that the regression curves of the three functions have the same change trend as the measured curves. However, compared with the exponential function and hyperbolic function, the logarithmic function has the highest fitting accuracy and its correlation coefficient can reach more than 0.97, while the exponential function has the worst fitting effect and the correlation coefficient is lower than 0.96.

Table 2 further presents the maximum error table of logarithmic function fitting for each section, in which the third and fourth columns represent the measured and fitted values corresponding to the maximum error respectively. As shown in Table 2, the maximum fitting error occurred in the DIK 159+018 section, which is 0.55 cm, and the corresponding error percentage is 9.36%. For the horizontal convergence and vault settlement in the construction process of ultra-shallow buried high-speed railway tunnel with broken surrounding rock, the logarithmic function fitting effect is good, the error is within 10%, and the fitting accuracy is higher than 90%.

Table 2. Maximum error for logarithmic function fitting

Item	Mileage	Measured (cm)	Fitted (cm)	Error (cm)	Percentage error (%)
Horizontal convergence of tunnel sidewalls	DIK 159+003	4.72	5.08	-0.36	7.63%
	DIK 159+018	5.90	5.45	0.55	9.36%
Settlement of tunnel vault	DIK 159+003	2.76	2.63	0.13	4.68%
	DIK 159+018	4.25	4.58	-0.33	-7.82%

5. Conclusions

Taking Huying Xishan tunnel as the engineering background, numerical simulation and field measurement methods are adopted to analyze the main deformation characteristics of ultra-shallow buried high-speed railway tunnel in broken surrounding rock during construction. The conclusions are as follows:

1. The stress concentration occurs at the boundary of tunnel sidewall and surrounding rock, and the vertical displacement of tunnel vault and bottom appears obviously.
2. The horizontal displacement on both sides of the initial lining is obvious, while the horizontal displacement on the upper and lower support is small. The maximum lateral displacement of the initial lining is 1.71 cm, while the maximum vault settlement of the lower invert is 9.3 cm.
3. In the process of ultra-shallow buried high-speed railway tunnel excavation, both the horizontal convergence and the vault settlement increase with time. The growth rate is large in the early stage and tends to be stable in the later stage.
4. Compared with exponential and hyperbolic functions, logarithmic function is most suitable for regression analysis of horizontal convergence and measured vault settlement data, and its fitting accuracy is higher than 90%.

Restricted by the high cost and energy of the field measurement, we only study the construction mechanical characteristics of one tunnel. To make the conclusion of this research more general, more studies should be carried out on high-speed railway tunnels in the future.

Acknowledgements

This work was funded by the Henan Province Key R & D and Promotion Project in 2121 (Science and Technology Research) (Grant Nos. 212102310090). The authors are grateful for the great support from Henan Province Key R & D and Promotion Project.

References

- [1] A.M. Skłodowska, M. Mitew-Czajewska, “The influence of electronic detonators on the quality of the tunnel excavation”, *Archives of Civil Engineering*, 2021, vol. 67, no. 3, pp. 333–349, DOI: [10.24425/ace.2021.138059](https://doi.org/10.24425/ace.2021.138059).
- [2] J.S. Zhang, Y.Z. Qi, “Research on the intelligent positioning method of tunnel excavation face”, *Archives of Civil Engineering*, 2022, vol. 68, no. 1, pp. 431–441, DOI: [10.24425/ace.2022.140178](https://doi.org/10.24425/ace.2022.140178).
- [3] W. Bogusz, T. Godlewski, A. Siemińska-Lewandowska, “Parameters used for prediction of settlement trough due to TBM tunnelling”, *Archives of Civil Engineering*, 2021, vol. 67, no. 4, pp. 351–367, DOI: [10.24425/ace.2021.138504](https://doi.org/10.24425/ace.2021.138504).
- [4] S. Suwansawat, H.H. Einstein, “Describing Settlement Troughs over Twin Tunnels Using a Superposition Technique”, *Journal of Geotechnical & Geoenvironmental Engineering*, 2007, vol. 133, no. 4, pp. 445–468, DOI: [10.1061/\(ASCE\)1090-0241\(2007\)133:4\(445\)](https://doi.org/10.1061/(ASCE)1090-0241(2007)133:4(445)).
- [5] D. Chapman, S. Ahn, D.V. Hunt, “Investigating ground movements caused by the construction of multiple tunnels in soft ground using laboratory model tests”, *Canadian Geotechnical Journal*, 2007, vol. 44, no. 6, pp. 631–643, DOI: [10.1139/t07-018](https://doi.org/10.1139/t07-018).
- [6] I. Kahoul, S. Yahyaoui, Y. Mehidi, Y. Khadri, “Shallow tunnel face stability analysis using finite elements”, *Scientific Bulletin of National Mining University*, 2021, no. 1, pp. 91–97, DOI: [10.33271/nvngu/2021-1/091](https://doi.org/10.33271/nvngu/2021-1/091).
- [7] *Code for Design of Railway Tunnel. TB10003-2016*. China Railway Publishing House, 2019.
- [8] O. Nývlt, S. Prívará, L. Ferkl, “Probabilistic risk assessment of highway tunnels”, *Tunnelling and Underground Space Technology*, 2011, vol. 26, no. 1, pp. 71–82, DOI: [10.1016/j.tust.2010.06.010](https://doi.org/10.1016/j.tust.2010.06.010).
- [9] S. Dalgıç, “The influence of weak rocks on excavation and support of the Beykoz Tunnel, Turkey”, *Engineering Geology*, 2000, vol. 58, no. 2, pp. 137–148, DOI: [10.1016/S0013-7952\(00\)00054-5](https://doi.org/10.1016/S0013-7952(00)00054-5).
- [10] F.-S. Jeng, M.-C. Weng, T.-H. Huang, M.-L. Lin, “Deformational characteristics of weak sandstone and impact to tunnel deformation”, *Tunnelling and Underground Space Technology*, 2002, vol. 17, no. 3, pp. 263–274, DOI: [10.1016/s0886-7798\(02\)00011-1](https://doi.org/10.1016/s0886-7798(02)00011-1).
- [11] Z.Q. Chen, C. He, G.W. Xu, et al., “Supporting mechanism and mechanical behavior of a double primary support method for tunnels in broken phyllite under high geo-stress: a case study”, *Bulletin of Engineering Geology and the Environment*, 2019, vol. 78, pp. 5253–5267, DOI: [10.1007/s10064-019-01479-1](https://doi.org/10.1007/s10064-019-01479-1).
- [12] M. Hisatake, Y. Hieda, “Three-dimensional back-analysis method for the mechanical parameters of the new ground ahead of a tunnel face”, *Tunnelling and Underground Space Technology*, 2008, vol. 23, no. 4, pp. 373–380, DOI: [10.1016/j.tust.2007.06.006](https://doi.org/10.1016/j.tust.2007.06.006).
- [13] A.S. Alagha, D.N. Chapman, “Numerical modelling of tunnel face stability in homogeneous and layered soft ground”, *Tunnelling and Underground Space Technology*, 2019, vol. 94, art. ID 103096, DOI: [10.1016/j.tust.2019.103096](https://doi.org/10.1016/j.tust.2019.103096).
- [14] Y. Shao, C. Yan, Q. Ma, “Analysis of the influence of fault fracture zone and dike on tunnel excavation”, *Journal of China and Foreign Highway*, 2015, vol. 35, no. 6, pp. 1–6, DOI: [10.14048/j.issn.1671-2579.2015.06.047](https://doi.org/10.14048/j.issn.1671-2579.2015.06.047).
- [15] Y. Wu, W. Wang, Q. Xu, et al., “Model test and numerical simulation of vault collapse in soft tunnel surrounding rock”, *Highway*, 2018, vol. 63, no. 6, pp. 1–6.
- [16] Q. Xu, P. Cheng, H. Zhu, et al., “Test and numerical simulation on stress disturbance characteristics of tunnel excavation in soft surrounding rock”, *Modern Tunnelling Technology*, 2016, no. 6, pp. 154–164, DOI: [10.13807/j.cnki.mtt.2016.06.021](https://doi.org/10.13807/j.cnki.mtt.2016.06.021).

Received: 22.03.2022, Revised: 14.05.2022